11th International Symposium on Turbulence and Shear Flow Phenomena (TSFP11)
Southampton, UK, July 30 to August 2, 2019

TURBULENT BOUNDARY LAYER DRAG REDUCTION USING PULSED-DC PLASMA ACTUATION

Alan Duong
Institute for Flow Physics and Control
University of Notre Dame
Notre Dame, IN, USA
Alan.H.Duong.9@nd.edu

Samaresh Midya
Institute for Flow Physics and Control
University of Notre Dame
Notre Dame, IN, USA
Samaresh.Midya.1@nd.edu

Thomas C. Corke
Institute for Flow Physics and Control
University of Notre Dame
Notre Dame, IN, USA
tcorke@nd.edul

Fazle Hussain
Mechanical Engineering
Texas Tech University
Lubbock, TX 79405
Fazle.Hussain@ttu.edu

Flint O. Thomas
Institute for Flow Physics and Control
University of Notre Dame
Notre Dame, IN, USA
fthomas@nd.edu

ABSTRACT

In this paper, we report on an active flow control approach that has produced unprecedented levels of turbulent boundary layer viscous drag reduction in excess of 70%. Furthermore, by incorporating a flush mounted, pulsed-DC plasma actuator array with exceedingly low power input, the power savings due to drag reduction has exceeded the power input. With regard to turbulence production mechanisms, the actuator gives rise to a reduction in the frequency of near-wall "burst-sweep" events that scales linearly with the wall shear stress. Mean velocity profiles indicate that the effect of the actuation in confined to the sublayer and buffer layer regions and the degree of drag reduction has been shown to scale with the number of low-speed streaks under simultaneous control.

Besides the obvious practical interest in this flow control approach, it also offers an opportunity to provide controlled initial conditions with which to investigate the response of the turbulent boundary layer turbulence generation mechanisms.

INTRODUCTION

The pursuit of viscous drag reduction in turbulent boundary layers began in the late 1970s and continues in earnest today as reviewed recently by Corke and Thomas (2018). Schoppa and Hussain (1998) proposed a large-scale strategy for skin friction drag reduction which was demonstrated in channel flow DNS. They imposed a streamwise-independent, near-wall spanwise velocity component along the channel wall by means of either a pair of counter-rotating streamwise vortices, or opposed wall jets. In either case, the amplitude of the spanwise control flow was only 6% of the channel centerline velocity and skin friction drag reductions of 20% and 50% were obtained for the counter-rotating vortices and spanwise opposed wall jets, respectively. In a subsequent work, Schoppa and Hussain (2002) showed that Streak Transient Growth (STG) can produce linear growth of streamwise disturbances that is an order-of-magnitude larger than normal-mode instability. In their view, the flow control in their DNS simultion served to prevent the lift-up of low-speed streaks, thereby limiting their flanking wall-normal vorticity component which, in their formulation, is a critical parameter for the self-sustaining cycle of wall turbulence generation.

Motivated, in part, by the above referenced work, exeperiments involving the active control of a zero pressure gradient (ZPG) turbulent boundary layer by means of flush mounted pulsed-DC plasma actuator arrays are presented.

THE PULSED-DC ACTUATOR ARRAY

The pulsed-DC dielectric barrier discharge (DBD) plasma actuator was used as the primary means of skin friction flow control. The geometric configuration of this pulsed-DC actuator is similar to that of a typical AC driven DBD actuator in that it has two staggered electrodes separated by a dielectric barrier material. However, as shown in Figure 1, in the pulsed-DC actuator, a common DC voltage is supplied to both surface and covered electrodes. The exposed electrode's applied voltage remains constant in time while the encapsulated electrode is periodically grounded for extremely short instances of time O (20 μs) via a solid state switch and is subsequently allowed to rise back to the supply voltage. This has the effect of producing a body force that gives rise to a compact wall jet as indicated in Figure 1. Figure 2 presents sample current and voltage-time histories for the pulsed-DC actuator. The pulse period was 500 Hz and the duty cycle was 1%. An important characteristic from an application standpoint is that, over most of the cycle, the current-voltage product is extremely small. The power supplied to the plasma actuator array was only 0.40 W/m, based on the total length of plasma formed in the actuator arrays used in the reported experiments.

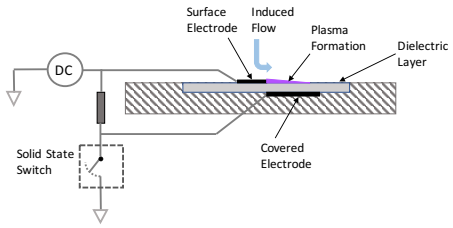

Figure 1. Schematic of the pulsed-DC actuator configuration.

Two types of pulsed-DC plasma actuator arrrays were constructed for the flow control experiments. In both types the surface electrodes were flush mounted and extended in the streamwise direction. The nature of the spanwise flow produced by the two configurations is shown schematically in Figure 3. In this figure the plasma forming region (shown in blue) occurs near the overlapping edge of the exposed electrode and resulted in a spanwise near-wall flow. Configuration A produced a unidirectional, spanwise near-wall velocity component while configuration B produced spatially periodic, opposed spanwise wall jets. In both cases the velocity produced by the actuators was on the order of the local friction velocity,

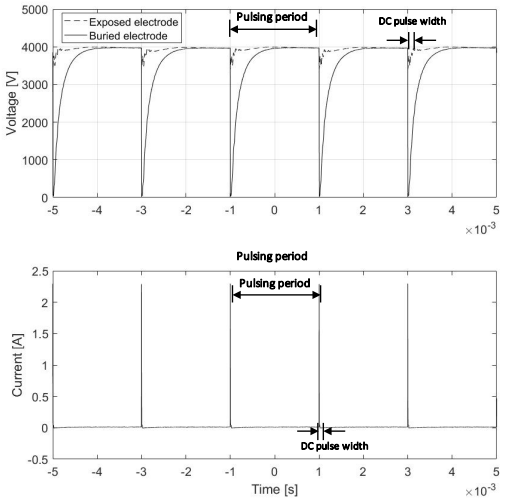

Figure 2. Sample pulsed-DC aactuator current and voltage time histories.

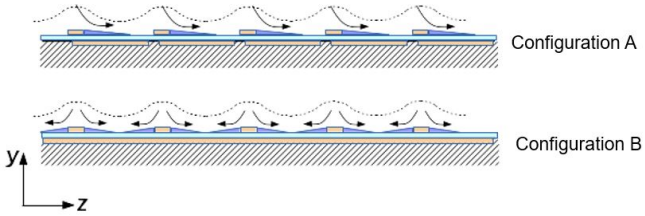

Figure 3. Pulsed-DC actuator array configurations: (A) uniform spanwise blowing and (B) spanwise opposed wall jets.

u_τ. The design objective of the actuator arrays was to produce a spanwise near-wall flow of sufficient magnitude to inhibit the lift-up of the low speed streaks.

The base of each actuator array test plate consisted of a honeycomb composite with a thin stainlesssteel skin that provides a rigid, flat base for the plasma actuator array. A 6.35 mm thick sheet of G11 Garolite was bonded to the top surface of the honeycomb plate to provide an electrically insulating layer. Each plasma actuator array was then built up on the surface of the Garolite sheet. The dielectric insulator was formed from a sheet of 0.102 mm thick mica. The mica sheet was glue-backed and covered the whole 22.86 cm. square test plate area. The pattern for the covered electrodes and their electrical connections was machined into the Garolite sheet surface. This produced a recess for each of the 0.1016 mm thick copper foil electrodes (0.0508 mm thick copper and 0.0508 mm thick adhesive layer) and the electrical connection between them that resulted in a smooth surface on which the dielectric film was applied. Exposed electrodes were also fabricated from the same copper foil tape. The pattern was applied to the exposed surface of the mica film. These were connected to a common electrical connection to uniformly distribute the power to the exposed electrodes.

EXPERIMENTAL FACILITY

The experiments were performed in the Mach 0.6 wind tunnel at the University of Notre Dame. The wind tunnel is a low-disturbance, closed-return wind tunnel with freestream air temperature control. Turbulence management consisting of a honeycomb section followed by five seamless, low-solidity screens woven from 0.19 mm diameter 316-stainless steel wire provides a very low turbulence intensity level throughout the Mach number range of the tunnel, $\sqrt{\overline{u^2}}/U_\infty < 0.05\%$. The test section dimensions are 1 m. by 1 m. cross-section and 3 m. in length. The freestream Mach number, M_∞, range for the first set of experiments presented in this paper was $0.05 \leq M_\infty \leq 0.15$ which corresponds to freestream velocities from 17.4 m/s to 52 m/s. This corresponds to an Re_θ range of $4538 \leq Re_\theta \leq 11{,}636$.

Friction drag was measured directly on a 22.86 cm square test plate located in the center of a removable Aluminum panel which was placed in one of the windows in the bottom wall of the test section. The test plate was either a smooth plate or one of the plasma actuator array types shown in Figure 3. The Aluminum panel was machined such that the gap around the test plate was no more than 0.508 mm. The test plate was mounted on a pair of linear air bearings that were fixed under the Aluminum panel within a sealed enclosure. The connection to the test plate was adjustable at four points so that the flow-side surface of the test plate is flush with the tunnel floor to within ±0.2 mm. The air bearings were aligned in the mean flow direction and provide a frictionless motion that was resisted by a translation load cell. The load cell used has a maximum rated output of 2 N (204 gm) and was chosen to have a high resolution across the range of experimental conditions. The load cell has a total uncertainty of 0.06% of the rated output or approximately 0.12 gm. The drag force on the test panel was expected to vary between 3 gm to 22 gm, therefore, the maximum uncertainty in the drag measurements was approximately 4% at the lowest speed and 0.06% at the highest speed. Verification of the experimental setup was done by comparing baseline drag measurements over a smooth plate to the canonical Coles-Fernholz relation for ZPG turbulent boundary layers. The same was done with the plasma actuator array in its unpowered state.

EXPERIMENTAL RESULTS

In this section drag reduction results for the actuator array producing unidirectional spanwise blowing (Configuration A) are presented. The actuator array voltage was varied from 4 – 8 kV, and the pulse frequency was fixed at 500 Hz. The unidirectional actuator was fabricated with a covered electrode width of 16 mm and a surface electrode width of 2 mm. The inter-electrode spacing was set to λ_z = 23 mm and the surface electrodes extended 7cm in the streamwise direction (15-19 boundary layer thicknesses over the Mach number range of the experiments). Figure 4 presents the percent change in measured drag as a function of applied actuator voltage for a Mach number range of $0.05 \leq M_\infty \leq 0.15$. Drag reduction in excess of 70% is indicated.

Figure 5 presents the drag reduction results for the 6, 7 and 8kV cases (which are highlighted in Figure 4), but presented as a function of the number of viscous wall units, $\lambda_z^+ \equiv \lambda_z u_\tau/\nu$, between adjacent surface electrodes. It is clear from Figure 5 that the degree of drag reduction at fixed actuator voltage scales on the number of near wall streaks under simultaneous control; the smaller the number of viscous wall units between surface electrodes, the greater the drag reduction. Peak drag reduction is observed to be associated with $\lambda_z^+ \approx 1000$ or the simultaneous control of approximatley10 low speed streaks. The reduced effectiveness of drag reduction with increase in Mach number at fixed voltage shown in Figure 4 is not an actuator authority issue. Rather, it is due to the increased number of streaks between surface electrodes as the Mach number increases. The logarithmic variation shown in Figure 5

indicates that the change in drag (per unit number of streaks) is inversely proportional to the number of streaks.

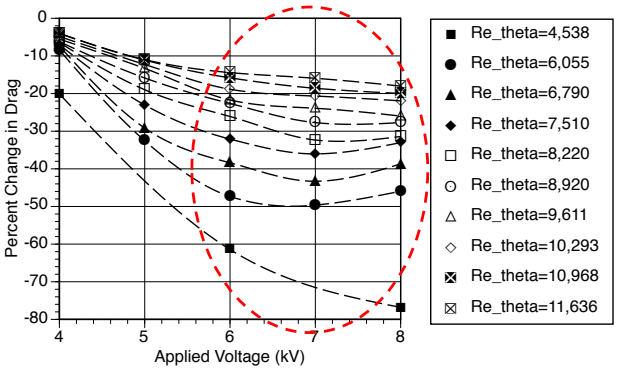

Figure 4. Percent change in drag as a function of actuator voltage. Unidirectional spanwise blowing actuator array.

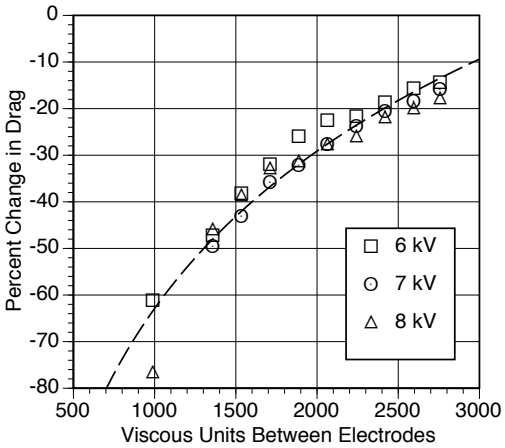

Figure 5. Percent change in drag as a function of the viscous wall units between electrodes (dashed line is a logarithmic fit).

Figure 6 presents the percent change in drag as a function of the maximum plasma-induced spanwise velocity, W_{max}, normalized by the local friction velocity for the base flow. The value of W_{max} as a function of applied voltage was obtained from glass pitot traverses under quiescent conditons. These measurements showed that the spanwise velocity decays exponentially with distance from the surface electrode. Figure 6 indicates that the degree of drag reduction is proportional to the amplitude of the plasma-induced spanwise flow which is $O(u_\tau)$.

Taken together, Figures 5 and 6 suggest that the degree of drag reduction achieved, ΔD, is a function of two parameters,

$$\Delta D = f(\lambda_z^+, W_{max}/u_\tau) \quad (1)$$

The first parameter is related to the number of streaks under simultaneous control and, in effect, provides the *potential* for drag reduction. The second "amplitude parameter" expressses the level of spanwise plasma-induced flow required relative to the local friction velocity.

Constant temperature hot-wire anemometry measurements were performed at a streamwise location 1 cm downstream of the plasma actuator array. These measurements utilized a custom fabricated, optically isolated circuit patterned after the design implemented by Wilkinson (2003). The anemometer output was frequency compensated to 10 kHz and digitally

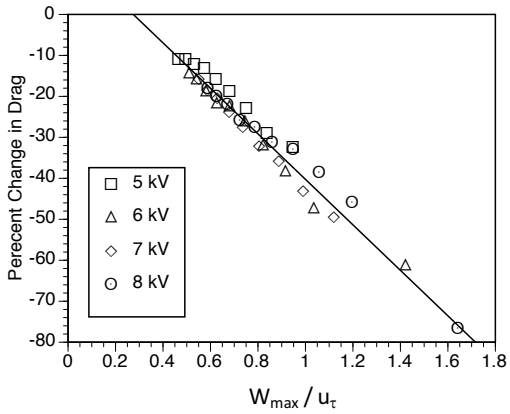

Figure 6. Percent change in drag as a function of the ratio of W_{max}/u_τ.

sampled at 25 kHz. As an example of the influence of the plasma actuation on the mean flow, Figure 7 presents a comparison between the outer variable scaled wall-normal mean velocity profiles with the plasma array both off and on at the Mach 0.05 freestream condition. Figure 7a shows the outer-variable scaled mean velocity over the full extent of the boundary layer. Based on this, there appears to be very little difference between the two conditions. However closer inspection near the wall, with $y/\delta < 0.02$ (corresponding to $y^+ < 41$ for the plasma off case) shown in Figure 7b, reveals a notable change. Specifically, the boundary layer with the plasma array operating exhibits a lower mean strain rate dU/dy that reflects the lower shear stress at the wall.

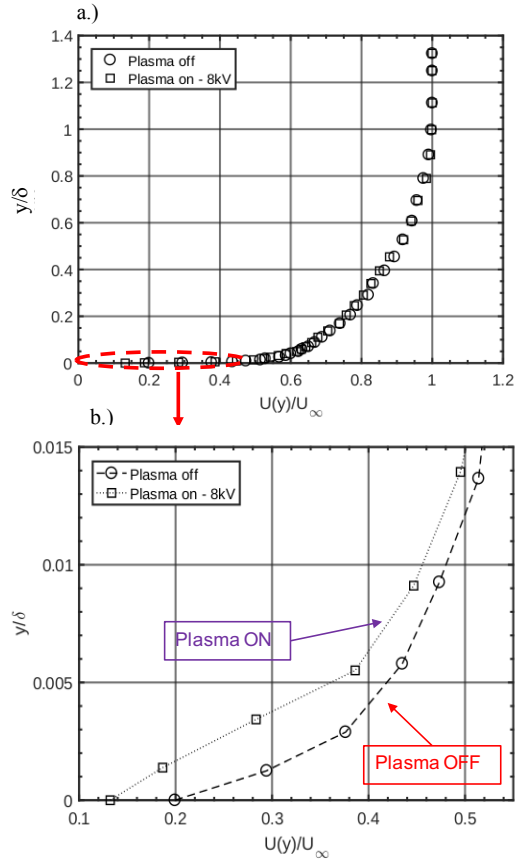

Figure 7. Mean velocity profiles showing (a) the full extent and (b) the near-wall region of the turbulent boundary layer for plasma off and on at 8kV for the $Re_\theta = 4538$ case.

In contrast to the influence on the mean flow, the streamwise velocity fluctuation levels were affected across the entire boundary layer as a result of the plasma actuation. This is demonstrated in Figure 8, which compares wall-normal profiles of turbulence intensity, $\sqrt{\overline{u^2}}/U_\infty$, with the plasma array operating and off for the same experimental conditions corresponding to Figure 7. These data indicate a reduction in the streamwise velocity fluctuation levels at all heights in the boundary layer when the drag was reduced by the plasma array with the largest reduction occurring near the wall. Similar results were obtained for all Reynolds number conditions. This aspect is further illustrated in Figure 9 which presents the ratio $\overline{u^2}_{plasma}/\overline{u^2}_{no\ plasma}$. This figure shows that most of the reduction in the turbulence fluctuation level with the plasma array operating occurs close to the wall, y/δ < 0.01. However, there is also a nearly constant turbulence reduction throughout the log layer with $\overline{u^2}_{plasma}/\overline{u^2}_{baseline} = 0.87$.

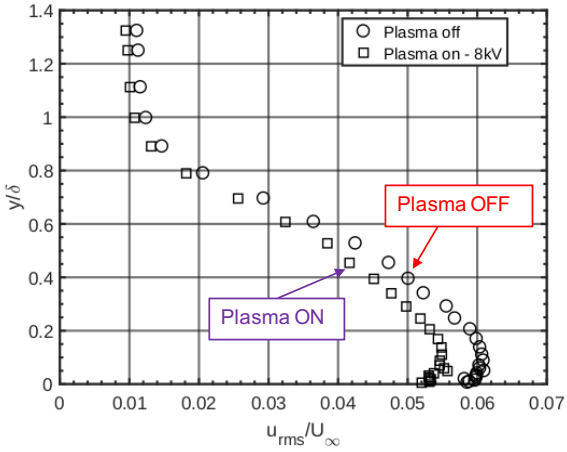

Figure 8. Comparison of wall-normal profiles of turbulence intensity for the plasma off and and on at 8kV for the Re_θ = 4538 case.

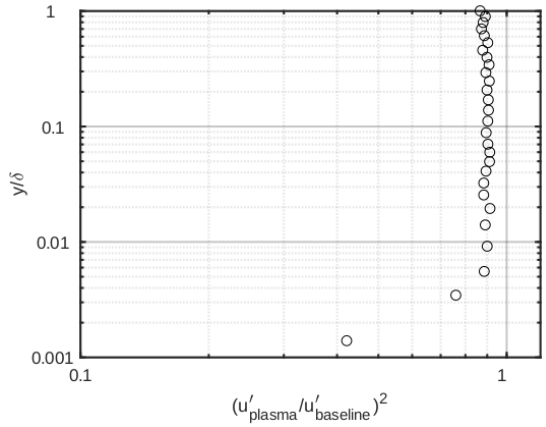

Figure 9. Wall-normal profiles of $\overline{u^2}_{plasma}/\overline{u^2}_{baseline}$ for the Re_θ = 4538 case.

Kline et. al (1967) noted a direct correlation between the "bursting frequency" associated with the lift-up and interaction of low-speed streaks with the outer flow and the wall shear stress. Given the large reduction in skin friction observed in the experiments it was of interst to examine the effect the pulsed-DC plasma actuation had on the character and frequency of low-speed ejection and sweep events. The Variable Interval Time Averging (VITA) technique as described by Blackwelder and Kaplan (1976) was utilized with the same threshold parameters. In each case, the VITA measurements presented were obtained at a wall-normal position of y^+=15 and were subsequently compared for both plasma on and off conditions.

Figure 10 shows a representative sample result from the VITA analysis which was performed across the full range of Mach numbers. The plot compares the conditional VITA signatures with and without plasma actuation at 8kV for the M= 0.05 case. An interesting observation from Figure 10 is that there is a significant difference in the local deceleration (ejection) portion of the signature. This ejection is associated with the "lift-up" of low-speed streaks. In contrast, the acceleration part of the VITA signature (sweep) is comparatively unaffected. The results from Figure 10 suggest that the spanwise near wall flow induced by the plasma actuator array serves to suppress streak lift-up. The VITA signature modification shown in Figure 10 was typical of those observed at all Mach numbers examined.

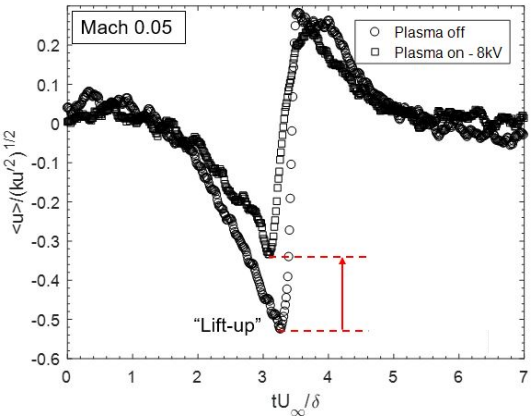

Figure 10. Comparison of VITA signatures with and without plasma actuation.

Figure 11 presents the probability distribution of the period between VITA events both with and without plasma flow control for the M= 0.05 case. As indicated in this figure (and in the other Mach number cases investigated), the total number of "burst" events detected decreased significantly when the plasma actuator array was operational and the average frequency between burst events decreased as a result. This indicates that the plasma actuator array had a direct impact on near-wall structures in the boundary layer which, in turn, influenced the friction drag that was measured.

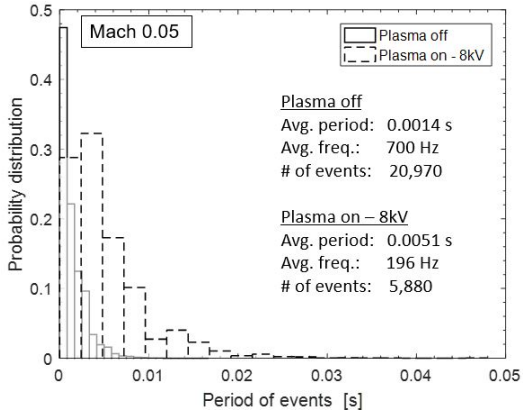

Figure 11. Probability distribution of the period between VITA events for the M= 0.05 case.

Figure 12 compares the number of "burst" events detected over a fixed period of time as a function of Re_θ with the plasma array off and operating. The dashed lines are linear best-fits through the two respective data sets. Also shown at each Re_θ is the difference in the number of burst events with plasma on and off. The plot clearly shows that the effect of the plasma array is to uniformly reduce the number of "burst" events occurring over the range of Reynolds numbers for the experiments.

A clear demonstration of the consistency between the reduction in the number of "burst" events and the reduction in drag produced by the plasma array is shown in Figure 13. This figure presents the percentage change in the number of "burst" events as a function of the percentage change in drag for different M_∞. For this figure, the percentage drag reduction is based on the results shown previously in Figure 4. The dashed line is a linear best-fit through the data. This demonstrates a nearly 1:1 correlation between the percent change in the number of "burst" events and the percent change in the viscous drag produced by the plasma array.

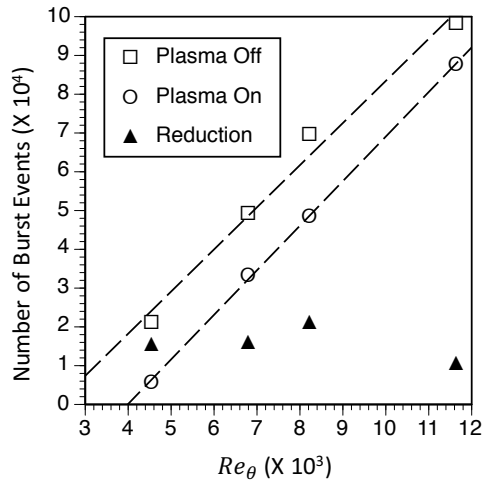

Figure 12. Number of burst events detected over a fixed period of time as a function of Re_θ for plasma array on and off.

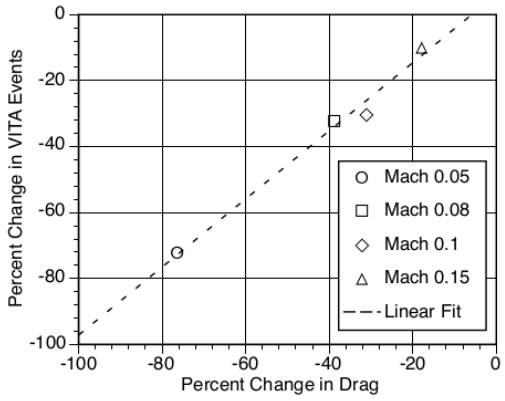

Figure 13. Percent change in the number of VITA events as a function of the percent change in drag.

Figure 14 compares mean velocity profiles for the baseline and plasma drag-reduced boundary layers obtained at Mach 0.1 and presented in inner variable scaling, u+ versus ln(y+). The friction velocity, u_τ, used for the inner variable scaling is based on direct drag measurements. The percent of drag reduction with the plasma array operating is also indicated. The line through the respective data corresponds to a best-fit to the logarithmic portion of the mean velocity profile and represents slope 1/κ. It is obvious from this comparison (and others not presented here) that the von Kármán coefficient, is decreased with drag reduction.

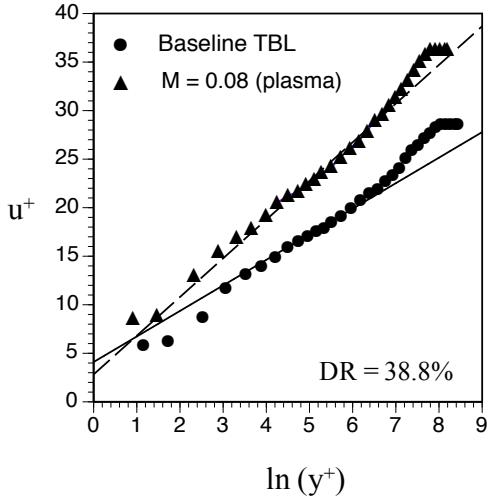

Figure 14. Sample comparison of inner-variable scaled mean velocity profiles using u_τ from the direct drag measurement.

Nagib & Chauhan (2008) documented consistent variations in the logarithmic mean velocity profile von Kármán coefficient for an extensive number of flows including turbulent boundary layers with adverse, zero and favorable streamwise pressure gradients, as well as channel and pipe flows. These data fell on a single empirical curve given as,

$$\kappa B = 1.6\left(e^{0.1663\,B}\text{-}1\right) \qquad (3)$$

where κ is the Kármán coefficient and B is the additive constant used in the logarithmic fit. Figure 15 presents values of κ and B obtained from the inner variable scaled mean velocity profiles obtained with the plasma actuator array operating over a range of approach Mach numbers. The empirical relation given in Equation 3 is shown by the solid curve. The intersection of the dashed vertical and horizontal lines correspond to the center of the zero-pressure gradient turbulent boundary layer data compiled by Nagib & Chauhan (2008). The baseline boundary layer cases in this study all fall very close to that intersection. The κ, B characteristics of the drag reduced boundary layers with different degrees of drag reduction are denoted by the different symbols. All of these are observed to lie very close to the empirical curve corresponding to adverse pressure gradient boundary layers. According to Nagib & Chauhan (2008), adverse pressure gradient boundary layers exhibit lower values of κ than zero or favorable pressure gradient boundary layers. Therefore, in the format of Figure 15, data from adverse pressure gradient boundary layers lie on the empirical curve below and to the left of data from zero pressure gradient boundary layers. That the values of κ and B for drag reduced boundary layers lie in this region is fully consistent with the reduced strain rate at the wall, with their location along the curve being in proportion to the degree of drag reduction.

DRAG REDUCTION AT HIGHER MACH NUMBERS

Additional drag reduction experiments were performed over a higher range of Mach numbers; from 0.30 to 0.50. For these experiments, the actuator design (in terms of spanwise inter-

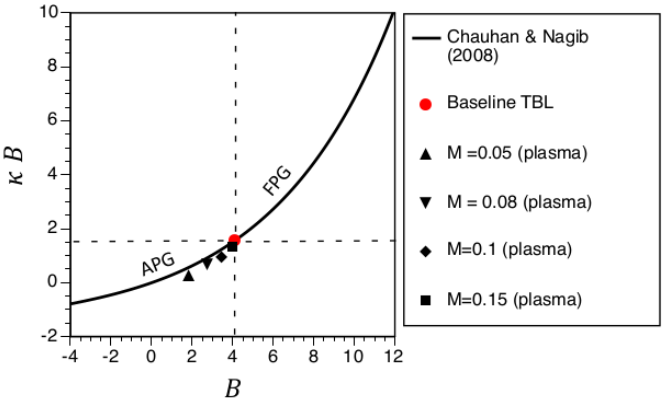

Figure 15. Comparison of baseline and plasma drag-reduced boundary layer values of κ and B with the empirical relation of Nagib and Chauhan (2008).

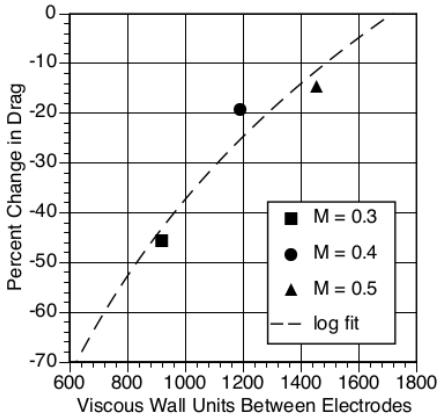

Figure 16. Percent change in drag as a function of λ_z^+ for the opposed wall jet actuator array operating at 8 kV for $0.3 \leq M_\infty \leq 0.5$. The dashed line is a log fit.

electrode spacing) was optimized for the turbulent boundary layer at M = 0.3. A λ_z = 4 mm spanwise electrode spacing was used that corresponded to λ_z^+ = 900 wall units. In contrast to the spanwise uniform blowing actuator array that was used for the previously presented results, the opposed wall jet design (Configuration B in Figure 3) was used because it more easily allows fabrication since the spacing of the electrodes becomes smaller to accommodate higher Mach number conditions. For these higher Mach number experiments the exposed electrodes were vapor deposited in copper to a thickness of 1 μm onto the mica dielectric sheet. This insured that the electrodes were completely within the boundary layer sublayer at the higher Mach numbers. This would not have been the case with the original copper foil tape used in the lower Mach number experiments. As in the experiments described previously, the plasma actuator array was operated with a pulsing frequency of 500 Hz, and a 1% duty cycle. The applied DC voltages ranged from 4-8kV. The drag was measured directly with the same floating element force balance with the only difference being that the load cells were exchanged for those rated for the larger drag forces that would occur at the higher Mach numbers.

The percent change in drag achieved with the opposed wall jet array operating at 8kV is shown in Figure 16 as a function of λ_z^+. As was the case for the unidirectional actuator operating at lower Mach numbers, the percent change in drag scales logarithmically with the number of viscous wall units between electrodes. A drag reduction of 46% is achieved for λ_z^+ = 900 which corresponds to the M = 0.3 condition.

CONCLUSION

The pulsed-DC actuator designs presented in this paper were motivated by the idea of creating a plasma-induced, spanwise, near-wall flow $O(u_\tau)$ that is just sufficient to prevent the lift-up of low-speed streaks which have been shown in previous studies to play a key role in wall bounded turbulent flows. The plasma actuator arrays consisted of a spanwise array of electrodes located on the wall surface and aligned with the mean flow direction. Actuator arrays producing either unidirectional spanwise blowing or a series of opposed wall jets have both achieved unprecedented levels of friction drag reduction in turbulent boundary layers in experiments over the Mach number range of from 0.05 – 0.5. For both array configurations operated at a fixed applied voltage, the level of drag reduction achieved varies logarithmically with $\lambda_z u_\tau/\nu$ with the largest observed drag reduction occurring for values between 900 – 1000. This is equivalent to the simultaneous control of 9-10 low speed streaks between adjacent surface electrodes. This does not necessarily represent the optimum possible drag reduction but corresponds to the minimum number of streaks under simultaneous control for the fixed inter-electrode spacing and flow conditions in the reported experiments. For a given value of $\lambda_z u_\tau/\nu$, the level of drag reduction achieved is shown to vary linearly with W_{max}/u_τ with typical values on the order of unity.

Hotwire measurements showed that plasma-induced changes in the mean velocity profiles were confined to the near wall region. Furthermore, the plasma drag reduction changed both the von Kármán and additive coefficients and comparison to the empirical relation of Nagib & Chauhan (2008) showed the drag reduced cases were consistent with those associated with canonical adverse pressure gradient turbulent boundary layers. Turbulence intensity profiles exhibited a decrease in fluctuation levels throughout the boundary layer, although the largest turbulence reductions occurred in the near-wall region.

A premise of the plasma actuator design for drag reduction was that it would reduce the spanwise mean flow distortion associated with the lift-up of low speed streaks. Consistent with this, conditional VITA measurements show a modification of the "lift-up" portion of the characteristic burst-sweep signature, and a reduction is burst frequency that is approximately 1:1 correlated with the measured reduction in friction drag.

REFERENCES

Blackwelder, R. F. and Kaplan, R. E., 1976, "On the wall structure oft he turbulent boundary layer," *J. Fluid Mech*., Vol. 76, 1, pp. 89-112.

Corke, T. C. and Thomas, F. O., 2018, "Active and Passive Turbulent Boundary-Layer Drag Reduction," *AIAA Journal*, Vol. 56, 10, pp. 3835-3847.

Kline, S. J., Reynolds, W. C., Schraub, F. A. & Runstadler, P. W., 1967,"The structure of turbulent boundary layers," *J. Fluid Mech.*, Vol. 30, 4, pp. 741-773.

Nagib, H. M. and Chauhan, K. A., 2008,"Variation of von Karman constant in canonical flows," *Phys. Fluids*, 20, 101518.

Schoppa, W. & Hussain, F., 1998, "A large-scale control strategy for drag reduction in turbulent boundary layers," *Phys. Fluids*, 10, 1049.

Schoppa, W. & Hussain, F., 2002, "Coherent structure generation in near wall turbulence," *J. Fluid Mech.*, 453, pp.57-108.

Wilkinson, S., 2003, "Investigation of an oscillating surface plasma for turbulent drag reduction," AIAA Paper 2003-1023.